Orphan spin operators enable the acquisition of multiple 2D and 3D magic angle spinning solid-state NMR spectra

T. Gopinath[1] and Gianluigi Veglia[1,2,a)]
[1]*Department of Biochemistry, Molecular Biology and Biophysics, University of Minnesota, Minneapolis, Minnesota 55455, USA*
[2]*Department of Chemistry, University of Minnesota, Minneapolis, Minnesota 55455, USA*

(Received 8 February 2013; accepted 15 April 2013; published online 10 May 2013)

We propose a general method that enables the acquisition of multiple 2D and 3D solid-state NMR spectra for U-^{13}C, ^{15}N-labeled proteins. This method, called MEIOSIS (Multiple ExperIments via Orphan SpIn operatorS), makes it possible to detect four coherence transfer pathways simultaneously, utilizing orphan (i.e., neglected) spin operators of nuclear spin polarization generated during ^{15}N-^{13}C cross polarization (CP). In the MEIOSIS experiments, two phase-encoded free-induction decays are decoded into independent nuclear polarization pathways using Hadamard transformations. As a proof of principle, we show the acquisition of multiple 2D and 3D spectra of U-^{13}C, ^{15}N-labeled microcrystalline ubiquitin. Hadamard decoding of CP coherences into multiple independent spin operators is a new concept in solid-state NMR and is extendable to many other multidimensional experiments. The MEIOSIS method will increase the throughput of solid-state NMR techniques for microcrystalline proteins, membrane proteins, and protein fibrils. © *2013 AIP Publishing LLC*. [http://dx.doi.org/10.1063/1.4803126]

INTRODUCTION

Solid-state NMR (ssNMR) is the method of choice for probing structure, dynamics, chemistry, and ligand binding of microcrystalline and membrane-bound proteins at the atomic resolution.[1] Sensitivity and resolution of the resonances (typically ^{1}H, ^{13}C, and ^{15}N) in multidimensional NMR spectra are fundamental requirements for protein structural analysis. In spite of the most recent progress, multidimensional ssNMR experiments still require many days or weeks of spectrometer time.

A central element in the ssNMR experiment is cross-polarization (CP), which enables the polarization transfer from high to low gyromagnetic ratio nuclei.[2] During CP, multiple spin nuclear excitation pathways are generated.[3] However, only selected spin operators are transformed into detectable coherences, whereas several other pathways are discarded. While in liquid-state NMR there are several pulse sequences designed to detect discarded coherences via dual receivers or phase cycling schemes,[4] in ssNMR there are only a few examples that utilize orphan (i.e., neglected) spin operators to boost sensitivity.[5–13] In general, classical ssNMR pulse sequences eliminate orphan spin operators of magnetization either using z-filters or phase cycling schemes that suppress the spectral artifacts arising from undesired coherence transfer pathways.[14] Recently, we proposed new pulse schemes to recover orphan spin operators originating from chemical shift or dipolar coupling Hamiltonians, and convert them into observable coherences to enhance the sensitivity of static ssNMR experiments.[5–8] For rotating solids, we developed the dual acquisition magic angle spinning (DUMAS) approach,[9,10] which uses simultaneous cross-polarization (SIM-CP) between ^{1}H, ^{13}C, and ^{15}N and enable the simultaneous acquisition of two 2D or 3D experiments.

In this article, we present a new method, MEIOSIS (Multiple ExperIments via Orphan SpIn operatorS) that enables one to simultaneously acquire multiple multidimensional NMR spectra of uniformly ^{13}C, ^{15}N-labeled proteins. This new method utilizes two elements that were instrumental for the DUMAS approach: SIM-CP and long-living ^{15}N polarization. However, MEIOSIS also exploits the residual magnetization of NCA or NCO from specific-CP to generate phase-encoded coherence pathways that are decoded into *four* independent spectra using Hadamard transformations. To demonstrate the power of this method, we simultaneously acquired four 2D experiments (DARR,[15] N(CA)CX, NCO, and CA(N)CO[16]) and three 3D experiments (NCACX, NCOCX, and CA(N)COCX[17,18]) on a U-^{13}C, ^{15}N-labeled microcrystalline ubiquitin. Hadamard decoding the coherences into multiple independent spin operators is a general concept in NMR and can be used to redesign many pulse sequences.

THEORY

The MEIOSIS method utilizes the polarization from four pathways generated during the specific-CP transfer between ^{15}N and ^{13}C nuclei. Not only does this new pulse scheme detect the transferred polarization from ^{15}N to ^{13}C and vice versa, but it also recovers the residual magnetization of ^{15}N and ^{13}C that is not transferred during the specific-CP. To encode the four different pathways, the ^{15}N specific-CP pulse scheme is implemented with a phase alternation (+x, −x), resulting to two explicit acquisitions for each scan. The four polarization pathways are then decoded via Hadamard processing into multiple 2D or 3D experiments.

a)Author to whom correspondence should be addressed. Electronic mail: vegli001@umn.edu

An example of a pulse sequence designed with this MEIOSIS scheme is reported in Fig. 1(a). After a 90° pulse on ^{1}H, a SIM-CP sequence transfers the magnetization from ^{1}H to ^{13}C and ^{15}N. A 90° pulse with phase ϕ_3 brings the ^{15}N magnetization in the z-direction, while ^{13}C magnetization evolves during t_1'. A pair of 90° pulses on ^{13}C and ^{15}N aligns the ^{13}C magnetization along z and tips the ^{15}N magnetization in the x-axis, whose chemical shift evolves during t_1'' under ^{1}H decoupling. A 90° pulse tilts the ^{13}C magnetization on the x-axis and a specific-CP[19] is applied between ^{15}N and ^{13}Cα. The MEIOSIS method enables one to recover residual magnetization during the bidirectional polarization transfer[9] from N to Cα and Cα to N (i.e., NCA/CAN transfer), which makes it possible to obtain multiple spectra simultaneously.

Encoding four independent polarization pathways

To understand the theoretical basis of this method, we analyze the CP dynamics for a two-spin system (N-CA) in the double quantum (DQ), and zero quantum (ZQ) sub-spaces.[3]

Let N_i and C_i^{α} (i = x, y, z) be the Pauli spin matrices for ^{15}N and $^{13}C^{\alpha}$ (or CA), respectively. In Fig. 1(a) at $t_1' = t_1'' = 0$, the density matrix prior to NCA/CAN transfer is given by

$$\rho(t_1 = 0) \propto a^{C_\alpha} \cdot C_x^{\alpha} + b^{N} \cdot N_x, \tag{1}$$

where the $a^{C\alpha}$ and b^{N} coefficients represent the initial ^{13}C and ^{15}N polarizations, respectively.

To describe the dipolar spin Hamiltonian during specific-CP of time τ, we consider on resonance continuous wave RF irradiations with phase +x on ^{13}C and phase +x on ^{15}N, and with RF amplitudes ω_{1C} and ω_{1N}, respectively. Under these conditions the Hamiltonian can be written as

$$H(\tau) = H_D(\tau) + H_{RF}, \tag{2}$$

where $H_D(\tau) = D(\tau) \cdot 2C_z^{\alpha} N_z$ and $H_{RF} = \omega_{1C} C_x^{\alpha} + \omega_{1N} N_x$, $D(\tau) = \sum_{n=\pm1,\pm2} D_n \cdot e^{in\omega_r \tau}$, $D_{\pm1} = d^1 \cdot e^{\pm i\gamma}$, $D_{\pm2} = d^2 \cdot e^{\pm i2\gamma}$, $d^1 = \frac{d}{2\sqrt{2}} \cdot \sin(2\beta)$, $d^2 = \frac{d}{4} \cdot \sin^2\beta$, and $d = -(\frac{\mu_0}{4\pi})(\frac{\gamma_C \cdot \gamma_N \cdot \hbar}{r^3})$.

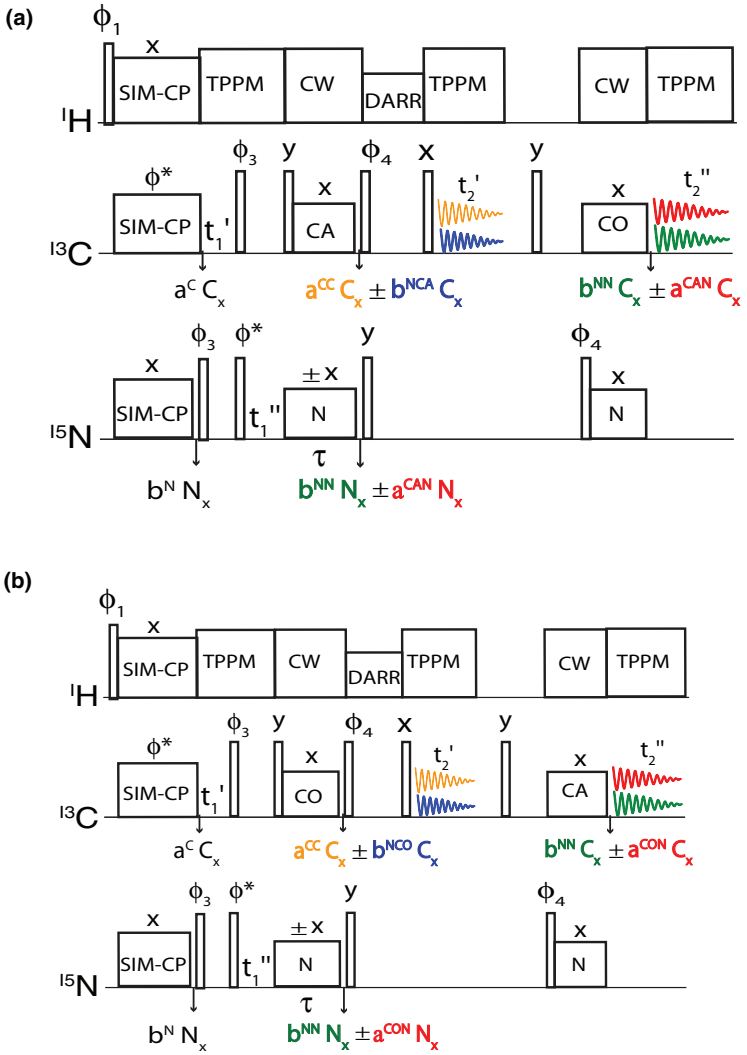

FIG. 1. (a) 2D MEIOSIS pulse sequence for simultaneous acquisition of four experiments: DARR, N(CA)CX, NCO, and CA(N)CO. (b) MEIOSIS pulse sequence with CON and CAN transfers inverted. The phase cycle of 2D MEIOSIS and conventional pulse sequences of Fig. 1S of the supplementary material[36] are given by: $\phi_1 = (y)_4, (-y)_4$, $\phi_2 = (x, x, -x, -x)_2$, $\phi_3 = (y, -y)_4$, $\phi_4 = (y, y, -y, -y)_2$, and $\phi_{rec} = (x, -x, -x, x, -x, x, x, -x)$. For indirect dimension, states mode acquisition is obtained by alternating the ϕ^* between x and y.

The angles β and γ describe the orientation of the internuclear vector with respect to the rotor frame, d is the ^{15}N-^{13}C dipolar coupling constant, and ω_r is the MAS spinning frequency. In a doubly tilted rotating (DTR) frame defined by the operator U_1, the resultant Hamiltonian and density matrix are given by H^T and ρ_+^T:

$$\begin{aligned} U_1 &= e^{-i\frac{\pi}{2}C_y^\alpha} \cdot e^{-i\frac{\pi}{2}N_y}, \\ H^T(\tau) &= D(\tau) \cdot 2C_x^\alpha N_x + \omega_{1C} C_z^\alpha + \omega_{1N} N_z, \\ \rho_+^T &\propto a^{C_\alpha} \cdot C_z^\alpha + b^N \cdot N_z, \end{aligned} \tag{3}$$

where the positive sign of ρ_+^T indicates the +x phase of ^{15}N spin lock during specific-CP. At the Hartmann-Hahn side band matching condition ($\omega_{1c} - \omega_{1N} = \pm\omega_r$ or $\pm 2\omega_r$), the dipolar recoupling can be represented by transforming the time-dependent Hamiltonian into a time-independent Hamiltonian in the interacting frame U_2:[19]

$$\begin{aligned} U_2 &= e^{-i\omega_{1C}C_z^\alpha\tau} \cdot e^{-i\omega_{1N}N_z\tau}, \\ \rho_+^{T^*} &= U_2^{-1} \cdot \rho^T \cdot U_2 = \rho^T, \\ H^{T^*} &= U_2^{-1} \cdot H^T \cdot U_2 = d^n \cdot e^{in\gamma} \cdot 2\left(C_x^\alpha N_x + C_y^\alpha N_y\right). \end{aligned} \tag{4}$$

To describe the density matrix evolution, we define the ZQ and DQ operators[3] as follows:

$$\begin{aligned} ZQ_x &= 2C_x^\alpha N_x + 2C_y^\alpha N_y,\ ZQ_y = 2C_y^\alpha N_x - 2C_x^\alpha N_y, \\ ZQ_z &= C_z^\alpha - N_z, \\ DQ_x &= 2C_x^\alpha N_x - 2C_y^\alpha N_y,\ DQ_y = 2C_y^\alpha N_x + 2C_x^\alpha N_y, \\ DQ_z &= C_z^\alpha + N_z. \end{aligned} \tag{5}$$

Therefore, the density matrix and Hamiltonian can be expressed as

$$\begin{aligned} \rho_+^T &\propto \frac{a^{C_\alpha}}{2}.(ZQ_z + DQ_z) - \frac{b^N}{2}.(ZQ_z - DQ_z), \\ H^{T^*} &= d^n.e^{in\gamma} \cdot ZQ_x. \end{aligned} \tag{6}$$

During the specific-CP sequence of time τ, the DQ_z term does not evolve under the Hamiltonian, while ZQ_z evolves into ZQ_y. For a specific crystalline orientation (defined by the β and γ angles), the NMR signal for $n = \pm 1$ matching conditions oscillates with a frequency d^1, and for $n = \pm 2$ with frequency d^2. The resultant density matrix for all crystal orientations can be written as

$$\begin{aligned} \rho_+^T \xrightarrow{H^{T^*}(\tau)} & \frac{1}{2}\sum_{\beta,\gamma} a^{C_\alpha}[ZQ_z\cos(d^n\cdot\tau) \\ & - ZQ_y\sin(d^n\cdot\tau) + DQ_z] \\ & - b^N[ZQ_z\cos(d^n\cdot\tau) - ZQ_y\sin(d^n\cdot\tau) - DQ_z]. \end{aligned} \tag{7}$$

A 90°_{-y} rotation (U_1^{-1}) is applied to back transform the operators from the DTR frame to the rotating frame. The latter converts the C_z^α and N_z of Eq. (7) into single quantum (SQ) operators C_x^α and N_x. Considering only the contribution of single spin operators, Eq. (7) can be written as

$$\begin{aligned} \rho_+(\tau) &\propto \sum_{\beta,\gamma} a^{C_\alpha} \cdot \left[C_x^\alpha \cos^2\left(d^n \cdot \frac{\tau}{2}\right) + N_x \sin^2\left(d^n \cdot \frac{\tau}{2}\right)\right] \\ &\quad + b^N \cdot \left[N_x \cos^2\left(d^n \cdot \frac{\tau}{2}\right) + C_x^\alpha \sin^2\left(d^n \cdot \frac{\tau}{2}\right)\right] \\ &\propto a^{CC} \cdot C_x^\alpha + a^{CAN} \cdot N_x + b^{NN} \cdot N_x + b^{NCA} \cdot C_x^\alpha, \end{aligned} \tag{8}$$

where a^{CC} and a^{CAN} represent the ^{13}Cα *residual* (i.e., not transferred to ^{15}N) and ^{15}N *transferred* (from ^{13}Cα to ^{15}N) magnetization resulting from all crystal orientations; while b^{NN} and b^{NCA} represent the ^{15}N residual and ^{13}Cα transferred magnetization, respectively. Although experimentally detectable (Fig. 2), the residual and transferred magnetization is difficult to quantify theoretically using a two-spin model. In fact, the oscillations of the operators for multiple-spin systems are attenuated by several factors, including the ^{13}C and ^{15}N homo- and hetero-nuclear dipolar coupling network, insufficient ^{1}H decoupling power, $T_{1\rho}$ relaxation, and RF inhomogeneity. Note that the density matrix in Eq. (8) is represented by *four* independent pathways encoded into single quantum coherences. After specific-CP, the polarization of four pathways is tilted along z direction by applying two 90° pulses on ^{15}N and ^{13}C. The longitudinal relaxation of ^{15}N is long-living on the order of a few seconds. Therefore, the ^{15}N polarization can be stored for several milliseconds without sensitivity loss. At the same time, the ^{13}C polarization of CC and NCA pathways undergoes homonuclear spin exchange during the DARR mixing time, which is then detected by a 90° readout pulse followed by t_2' acquisition. At zero DARR mixing period and $t_2' = 0$, the density matrix becomes

$$\rho_+ \propto \left(a^{CC} \cdot C_x^\alpha + b^{NCA} \cdot C_x^\alpha\right)_{1st-acq} + \left(b^{NN}N_z + a^{CAN}N_z\right). \tag{9}$$

The first term of Eq. (9) is acquired during t_2', while the second term representing the ^{15}N magnetization is stored along z. After the first acquisition, any longitudinal or transverse ^{13}C magnetization is suppressed by a 3 ms period followed by a 90° pulse and another 3 ms period. At this point, a 90° pulse on ^{15}N followed by NCO specific-CP transfers the magnetization from ^{15}N to ^{13}C′. The magnetization of both CAN and NN pathways is transferred to ^{13}C′, which is recorded during the second acquisition period t_2''. The resultant density matrix (ρ_+) for each scan is the sum of two density matrices associated with 1st and 2nd acquisitions that are recorded in two different memory locations:

$$\begin{aligned} \rho_+ &\propto \left(a^{CC}C_x^\alpha + b^{NCA}C_x^\alpha\right)_{1st-acqu} \\ &\quad + \left(b^{NN^*}C_x' + a^{CAN^*}C_x'\right)_{2nd-acq} \\ &\propto \left(\rho^{CC} + \rho^{NCA}\right)_{1st-acqu} + \left(\rho^{NN^*} + \rho^{CAN^*}\right)_{2nd-acqu}. \end{aligned} \tag{10}$$

Due to the second specific-CP, the amplitudes of the spin operators a^{CAN} and a^{NN} are reduced by a factor of 2–3 and are marked with an asterisk in Eq. (10).[18] In order to encode the operators of the density matrix in each acquisition, we

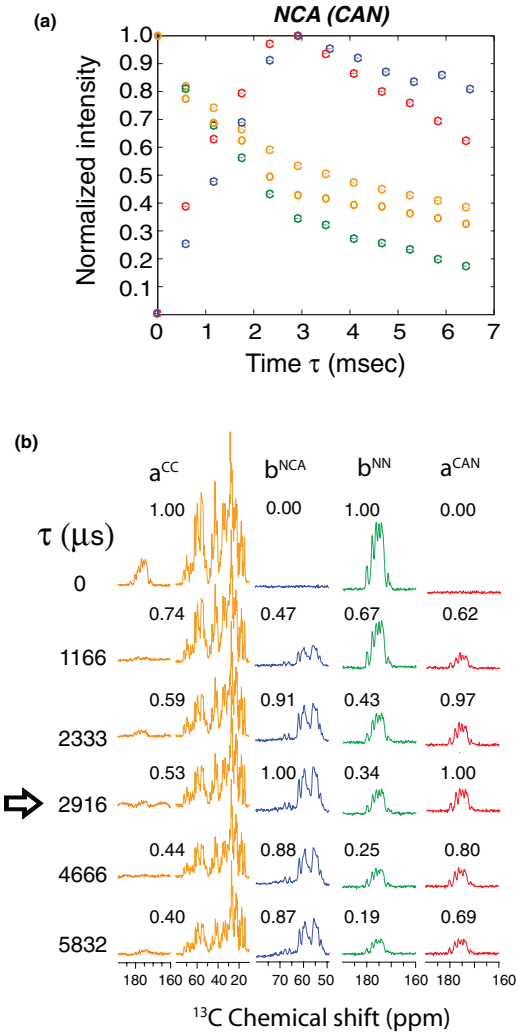

FIG. 2. (a) Experimental plot of ubiquitin showing the normalized intensities of four pathways during NCA (or CAN) transfer, as a function of specific-CP contact time (τ). Each data point is obtained by integrated intensities of the 1D spectra shown in (b), by using the pulse sequence of Fig. 1(a) with t_1', t_1'', and DARR mixing period set to zero. The maximum intensity of each pathway is normalized to one. The data points (a) and the corresponding spectra in (b) are color-coded according to respective pathways shown in Fig. 1. Open and closed orange colored circles indicate Cα (50–75 ppm) and aliphatic carbon region (0–75 ppm) intensities. The arrow indicates the optimal contact time (2916 μs) for maximum NCA and CAN transfer. The residual magnetization at 2916 μs corresponds to ∼34% for ^{15}N and ∼43% for the ^{13}Cα (50–75 ppm) and 54% for ^{13}C aliphatic (0–75 ppm) resonances. The residual magnetization of C′ region is less than 5% due to insufficient spin lock field.

record another scan with the phase of the ^{15}N RF flipped to −x during first specific-CP, while that of ^{13}C is kept at +x. The phase flip can either be incorporated in to Hamiltonian or in the initial density matrix. In the latter case, the operator formalisms of ZQ_z and DQ_z are inverted, and they become ($C_z + N_z$) and ($C_z - N_z$), respectively. By substituting these operators in Eq. (7) and considering only SQ coherences, the resultant density matrix, ρ_2, is

$$\begin{aligned}\rho_-(\tau) \propto & \sum_\gamma 2a^{C_\alpha}\left[C_x^\alpha \cos^2(d^n\tau) - N_x \sin^2(d^n\tau)\right] \\ & +2b^N\left[N_x \cos^2(d^n\tau) - C_x^\alpha \sin^2(d^n\tau)\right] \\ & \propto a^{CC}C_x^\alpha - a^{CAN}N_x + b^{NN}N_x - b^{NCA}C_x^\alpha. \quad (11)\end{aligned}$$

In analogy with Eqs. (8)–(10), the resultant density matrix of two acquisitions is given by

$$\begin{aligned}\rho_- \propto & \left(a^{CC}C_x^\alpha - b^{NCA}C_x^\alpha\right)_{1st-acqu} \\ & +\left(b^{NN^*}C_x' - a^{CAN^*}C_x'\right)_{2nd-acq} \\ & \propto (\rho^{CC} - \rho^{NCA})_{1st-acqu} + (\rho^{NN^*} - \rho^{CAN^*})_{2nd-acqu}. \quad (12)\end{aligned}$$

As for Eq. (10), the first acquisition in Eq. (12) gives the ^{13}C spectrum resulting from NCA and CC pathways, but with an inverted sign for the NCA transfer, and the second acquisition gives NN and CAN pathways, with an inverted sign for the CAN pathway. The free-induction decay (FID) signals ($G_\pm$) of the corresponding density matrices ($\rho\pm$) can be calculated as follows:

$$\begin{aligned}\rho_\pm(t_2', t_2'') \propto & \left[\rho^{CC}(t_2') \pm \rho^{NCA}(t_2')\right]_{1st-acqu} \\ & +\left[\rho^{NN^*}(t_2'') \pm \rho^{CAN^*}(t_2'')\right]_{2nd-acqu}, \quad (13) \\ G_\pm \propto & Tr\left[C_x \cdot \rho_\pm(t_2', t_2'')\right].\end{aligned}$$

Decoding the four independent pathways

In order to decode the four spin operators (CC, NCA, NN, and CAN, Fig. 1(a)), we need to consider the signs of four operators (Eqs. (10)–(13)) that resemble the rows of the four-dimensional Hadamard matrix. For the ^{15}N spin-lock with phase +x (Eq. (10)), the density matrices are $+\rho^{CC}$, $+\rho^{NCA}$, $+\rho^{NN}$, and $+\rho^{CAN}$; while for the −x phase (Eq. (12)) the density matrices are $+\rho^{CC}$, $-\rho^{NCA}$, $+\rho^{NN}$, and $-\rho^{CAN}$. By summing the two data sets in the first acquisition, the two CC components are added, while the NCA operator cancels out. On the other hand, by subtracting the two data sets, the NCA transfer corresponds to the sum of the two NCA components, while the CC operator cancels out. Similarly, the addition and subtraction of two data sets for the second acquisition will give magnetization resulting from NN and CAN pathways, respectively. The decoded FID signal can be calculated as follows:

$$\begin{aligned}G_{sum} = G_+ + G_- = & Tr\left\{\left[2C_x \cdot \rho^{CC}(t_2')\right]_{1st-acqu}\right. \\ & \left.+\left[2C_x \cdot \rho^{NN^*}(t_2'')\right]_{2nd-acqu}\right\}, \\ G_{diff} = G_+ - G_- = & Tr\left\{\left[2C_x \cdot \rho^{NCA}(t_2')\right]_{1st-acqu}\right. \\ & \left.+\left[2C_x \cdot \rho^{CAN^*}(t_2'')\right]_{2nd-acqu}\right\}. \quad (14)\end{aligned}$$

Note that G_{sum} and G_{diff} are decoded FID signals of two separate scans, G+ and G−.

For a 2D experiment with evolution time t_1' or t_1'' and ^{13}C homonuclear spin exchange during DARR mixing period, the

density matrices become

$$G_{sum} = G_+ + G_- = \sum_i Tr\left\{\left[2C_{ix}\cdot\rho_i^{CC}(t_2',\ t_2')\right]_{1st\text{-}acqu}^{DARR} + \left[2C_{ix}\cdot\rho_i^{NN^*}(t_1'',\ t_2'')\right]_{2nd\text{-}acqu}^{NCO}\right\},$$
$$G_{diff} = G_+ - G_- = \sum_i Tr\left\{\left[2C_{ix}\cdot\rho_i^{NCA}(t_1'',\ t_2')\right]_{1st\text{-}acqu}^{NCACX} + \left[2C_{x}\cdot\rho_i^{CAN^*}(t_1',\ t_2'')\right]_{2nd\text{-}acqu}^{CANCO}\right\}, \quad (15)$$

where the summation index i represents each of the ith carbon spins that contribute to the signal.

In the above theoretical treatment, during NCA/CAN transfer we considered the residual magnetization for $^{13}C\alpha$ and ^{15}N only. However, as will be shown in the Results and Discussion section, in addition to Cα one can also obtain the residual magnetization for the carbonyl and side chain carbons. In other words, there will be a CC pathway associated with backbone and side-chain carbon atoms that will contribute to the DARR spectrum.

The 2D MEIOSIS method (Fig. 1(a)) can be extended to 3D experiments (Fig. 4(a)) by incorporating an additional ^{13}C evolution period prior to the first and second acquisitions. Three 3D experiments, NCACX, NCOCX, and CA(N)COCX, are obtained from NCA, NN, and CAN pathways, respectively (Fig. 2). The ^{15}N t_1' evolutions of NCACX and NCOCX are synchronized with $^{13}C\alpha$ t_1'' of CA(N)COCX, whereas $^{13}C\alpha$ t_2' evolution of NCACX is synchronized with ^{13}CO t_2'' evolution of CA(N)COCX and NCOCX. Unlike 2D MEIOSIS, in the 3D experiment the residual ^{13}C magnetization a^{CC} is discarded. In fact, the chemical shift of the CC pathway evolves similarly during t_1' and t_2', and at longer dwell times gives an aliased 2D DARR spectrum along the 2D plane formed by F1′-F2′ diagonal and F3 axis.

RESULTS AND DISCUSSION

To analyze the amplitudes of the four pathways as a function of NCA/CAN specific-CP contact time, we carried out a series of 1D experiments on U-^{13}C, ^{15}N ubiquitin using the pulse sequence shown in Fig. 1(a) without DARR mixing period, and t_1' and t_1'' set to zero. Fig. 2 shows the amplitudes of the four pathways obtained from the integrated intensities of the 1D spectra at various specific-CP contact times. The data points and corresponding spectra in Figs. 2(a) and 2(b) are color-coded according to the individual pathways. The maximum of the NCA/CAN transfer occurs at approximately 3 ms contact time, and the residual magnetization corresponds to ∼34% for ^{15}N, ∼43% for the $^{13}C\alpha$ (50–75 ppm). Remarkably, the residual magnetization of the ^{13}C aliphatic (0–75 ppm) resonances is ∼53%! During the NCA/CAN transfer, the ^{13}C spin-lock sequence creates an effective field on the Cα region, while the carbonyl magnetization dephases due to insufficient RF amplitude of the spin-lock. Hence, the residual magnetization for $^{13}C'$ resonances is less than 5% (Fig. 2(b)). At the end of the τ period, all of the ^{13}C resonances should be encoded into the C_x spin operators (Eq. (8)). However, we detected a small C_y component (∼5%) for resonances in the frequency range corresponding to 0–30 ppm, which gives mixed phase (absorptive and dispersive) line shapes. The latter is due to an offset-dependent evolution of the magnetization during ^{13}C spin-lock field applied at 60 ppm. To eliminate this out-of-phase C_y component, we applied a phase cycle ϕ_4, which allows the acquisition of pure absorptive lines. Note that in 2D experiments phase cycle ϕ_4 is not required as the DARR mixing period suppresses the C_y components.

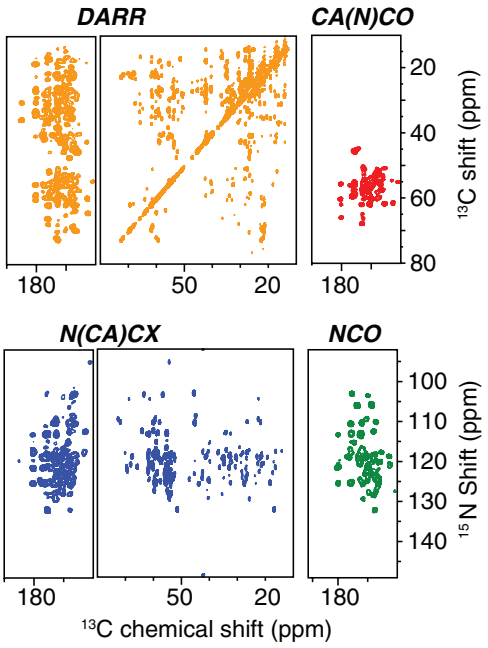

FIG. 3. Simultaneous acquisition of four 2D spectra using the MEIOSIS pulse sequence reported in Fig. 1(a).

We tested the 2D MEIOSIS pulse sequence for the simultaneous acquisition of four 2D spectra of U-^{15}N,^{13}C labeled sample of microcrystalline ubiquitin (Fig. 3) and compared the results with conventional experiments (Fig. 1S of the supplementary material).[36] The total experimental time for conventional experiments was ∼62 h, with DARR and NCACX experiments lasting 7 and 22 h, respectively, and NCO and CA(N)CO experiments 3.5 and 28 h, respectively (Fig. 2S of the supplementary material).[36] Remarkably, the total experimental time for the four experiments acquired simultaneously with the MEIOSIS sequence was ∼29 h, cutting experimental time by more than 50%. The sensitivity of each of the four spectra obtained from MEIOSIS is similar to the corresponding conventional experiments, as demonstrated in both the 1D spectra and contour plots reported in Fig. 3S of the supplementary material.[36]

The MEIOSIS experiment requires the optimization of indirect evolution times, taking into account both sensitivity and resolution of individual experiments. In 2D MEIOSIS, for instance, the t_1' evolution for DARR and CA(N)CO are time shared, therefore, the indirect spectral widths for these two spectra are identical. Note that it is possible to reduce the spectral width in the F_1' dimension (frequency domain of t_1') by taking into account the aliasing of carbonyl resonances of the DARR spectrum. The ^{13}C spectral width of DARR and CA(N)CO can be reduced by increasing the dwell time to 60–80 μs. The reduced ^{13}C spectral width in the DARR

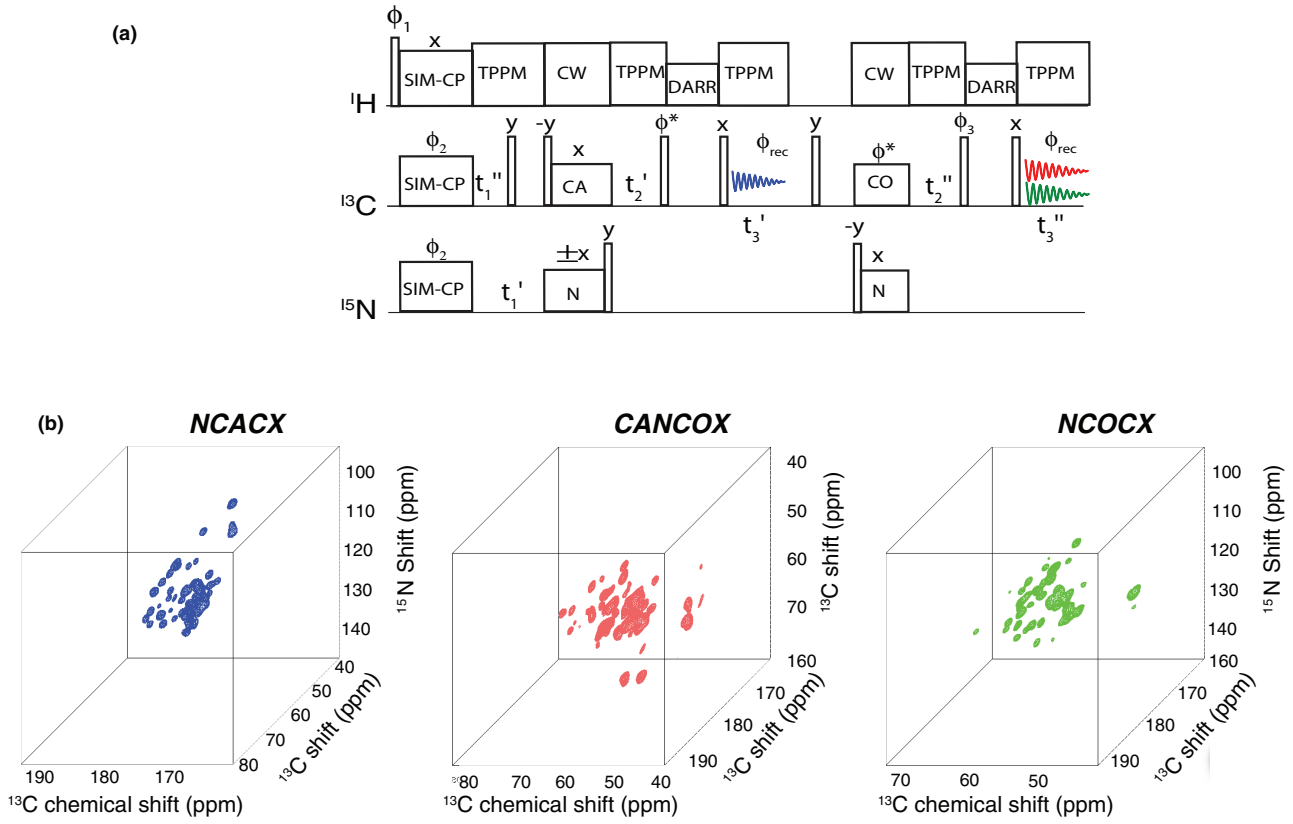

FIG. 4. Three-dimensional MEIOSIS pulse sequence for simultaneous acquisition of three 3D spectra: NCACX, NCOCX, and CAN(CO)CX. The phase cycle is given by $\phi_1 = (y, -y)_2$, $\phi_2 = x, x, -x, -x$, and $\phi_{rec} = x, -x, -x, x$. Sates mode acquisition of indirect dimensions is obtained by alternating ϕ_2, and ϕ^* phases between x and y.

experiment can be a significant advantage for MEIOSIS experiments, as during NCA specific-CP the residual magnetization of ^{13}CO as well as aromatic resonances is reduced to ∼5% of total intensity (Fig. 2), which leads to negligible aliased peaks. However, for accurate comparison between conventional and 2D MEIOSIS experiments we used the full ^{13}C spectral width (0–185 ppm) during t_1'.

The MEIOSIS scheme of Fig. 1(a) can also be reversed by setting the first and second specific-CP to NCO and NCA transfers, respectively (Fig. 1(b)). The resultant experiment allows simultaneous acquisition of the DARR, N(CO)CX, CO(N)CA, and NCA experiments. In the absence of DARR mixing time, the experimental amplitudes for the four pathways in the NCO/CON transfer with $t_1' = t_1'' = 0$, are shown in Fig. 4S of the supplementary material.[36] The NCO/CON transfer, however, requires higher RF amplitudes for ^{13}C ($7/2\omega_r$ = 45.5 kHz) compared to the NCA/CAN transfer ($3/2\omega_r$ = 19.5 kHz), and the ^{13}C offset is now centered at the carbonyl region. As shown in Fig. 4S of the supplementary material,[36] the residual magnetization for ^{13}C is ∼53% for the Cα region (50–75 ppm) and 46% for the aliphatic resonances (0–75 ppm), while the residual ^{15}N magnetization is ∼33%. In contrast to NCA/CAN transfer, the residual ^{13}CO magnetization of NCO/CON is about 40%.

The sensitivity of multidimensional ssNMR experiments decreases for longer DARR mixing periods. On the other hand, different DARR mixing periods are necessary to obtain short-, medium-, and long-range correlations for structure determination. Of course, it is preferable to combine experiments that are equally sensitive. Unfortunately the sensitivity for a given experiment depends on the building blocks used in the pulse sequence. The sensitivity of MEIOSIS experiments needs to be optimized using 1D spectra. For instance, as shown in Fig. 2, the intensity of the initial magnetization for CC and NCA pathways during the first acquisition is higher than that of the corresponding NN and CAN pathways detected during the second acquisition. Therefore, we designed the pulse sequence in such a way as to avoid a DARR mixing period prior to the second acquisition, finding the best compromise of sensitivity for the two acquisitions. However, it is possible to optimize the sensitivity of the experiments by applying a longer mixing period prior to the first acquisition (∼100 ms) and a much shorter mixing period (20 ms) prior to the second acquisition. In the latter case, we would obtain a MEIOSIS experiment consisting of four 2D spectra: DARR, N(CA)CX, CA(NCO)CX,[17] and N(CO)CX. Fig. 4(b) shows the 3D spectra NCACX, NCOCX, and CA(N)COCX acquired simultaneously using the 3D MEIOSIS pulse sequence shown in Fig. 4(a). The total acquisition time was 5 days.

The existence of residual ^{1}H polarization after ^{1}H-^{13}C CP was first identified by Pines and co-workers[20] to enhance the sensitivity of 1D ^{13}C spectra. However, this method requires the use of repetitive CP and continuous wave decoupling during the acquisition, giving poor resolution of the resonances. Later on, the ^{1}H residual polarization was also

described qualitatively by Levitt and co-workers.[3] In our implementation, we transform orphan spin operators into detectable coherences to either simultaneously acquire multiple experiments or to enhance the sensitivity of a single multidimensional experiment, thereby dramatically reducing the experimental time. We group these experiments in a category called polarization optimized experiments (POE). In static ssNMR, we designed POE to recover chemical shift or dipolar coupling coherences and convert them into observable terms to enhance the sensitivity of heteronuclear correlations (HETCOR) or separated local field experiments such as PISEMA (polarization inversion spin exchange at magic angle).[5–8,21] We also developed the DUMAS approach,[9,10] which consists of using SIM-CP between ^{1}H, ^{13}C, and ^{15}N to store and utilize ^{15}N magnetization, thus obtaining the simultaneous acquisition of two 2D experiments. Moreover, we discovered the possibility of transferring the magnetization simultaneously between ^{15}N and ^{13}Cα (or ^{13}C$'$) and vice versa for the acquisition of two 3D experiments concurrently. The MEIOSIS method was developed using the POE philosophy, i.e., making the best out of nuclear polarization. Unlike classical ssNMR methods (including DUMAS), MEIOSIS exploits four different polarization pathways that are transformed into four individual spectra. We anticipate that several other orphan spin operators can be rescued using this approach, such as those generated by CP between HC or HN nuclei in protonated and perdeuterated samples. In fact, the specific-CP scheme is used in almost all ^{13}C detected triple resonance experiments. Since the MEIOSIS scheme relies upon its ability to recover the lost polarization generated during specific-CP, this method is applicable to a multitude of pulse sequences. Moreover, variants of MEIOSIS could be designed using other homonuclear spin exchange schemes, such as DREAM (dipolar recoupling enhanced by amplitude modulation),[22] SPC5 (supercycled POST-C5),[23] PAR (proton assisted recoupling),[24] etc. Additionally, although we assessed the performance of MEIOSIS for specific-CP ^{15}N-^{13}C transfer, we anticipate that it could also be extended to other ^{15}N-^{13}C polarization transfer schemes such as symmetry based transfer sequences,[25] PAIN-CP (proton assisted insensitive nuclei cross polarization), as well as optimal control based NC transfer.[26,27] As recently demonstrated for the DUMAS methods,[28] we anticipate that the variants of MEIOSIS pulse schemes will be implemented for the structural analysis of U-^{2}H, ^{13}C, ^{15}N proteins with ^{1}H and ^{13}C dual-receiver acquisition.

CONCLUSIONS

In conclusion, we present a new, powerful method that allows one to recover lost polarization in classical experiments using Hadamard decoding. We have demonstrated this approach for four of the most common pulse sequences used for structure determination. The 2D MEIOSIS experiments will enable rapid scanning of protein sample conditions and monitor ligand binding on multiple chemical groups, simultaneously. 3D MEIOSIS will dramatically reduce acquisition time for backbone and side chain assignments. Additionally, the concepts presented in this paper open up the possibility of developing a new class of multidimensional ssNMR experiments for higher dimensionality, thus speeding up the structure determination of biomacromolecules. MEIOSIS can also be applied with faster spinning speeds[29] and/or perdeuteration.[30] When applied in concert with other fast acquisition and sensitivity enhancement techniques (e.g., dynamic nuclear polarization,[31] paramagnetic relaxation enhancements,[32] and ^{1}H detection[33]), this approach will dramatically increase the throughput of high-resolution structure determination by MAS ssNMR.

MATERIALS AND METHODS

All of the NMR experiments were performed using a VNMRS spectrometer operating at a ^{1}H Larmor frequency of 600 MHz. About 5 mg of U-^{13}C, ^{15}N ubiquitin was used to prepare the microcrystalline sample, which was then packed into a 3.2 mm rotor of BioMAS probe. A spinning rate (ω_r) of 13 kHz was used for all of the experiments, and the temperature was held constant at 5 °C. ^{15}N RF carrier frequency was centered at 120 ppm, while ^{13}C was centered at 100 ppm. The 90° pulse lengths for ^{1}H, ^{13}C, and ^{15}N were 2.5, 6, and 6 μs, respectively. During SIM-CP ^{13}C and ^{15}N RF amplitudes were set to 35 kHz, whereas ^{1}H RF amplitude was linearly ramped from 80% to 100% with the center of the slope set at 61 kHz. Based on the 1D calibration spectra, the Hartmann-Hahn contact time during SIM-CP was set to 300 μs. The sensitivity of ^{15}N SIM-CP spectrum is 90% of that of double resonance CP, whereas ^{13}C sensitivity is similar for CP and SIM-CP. It is to be noted that at higher spinning speeds (~20 kHz) the sensitivity of ^{13}C and ^{15}N SIM-CP is almost identical to that of double resonance CP.[34] For specific-CP from ^{15}N to ^{13}Cα (or ^{13}C$'$), the ^{13}C offset was shifted to 60 (or 177) ppm. During specific-CP, the ^{15}N RF amplitude was set to $(5/2)\cdot\omega_r = 32.5$ kHz, whereas ^{13}C RF amplitude was set to $(3/2)\cdot\omega_r$ (=19.5 kHz) and $(7/2)\cdot\omega_r$ (=45.5 kHz) for ^{13}Cα and ^{13}C$'$ transfers, respectively. The specific-CP was implemented with an adiabatic ramp ($\Delta \sim 1.6$ kHz and $\beta = 0.5$ kHz). The specific-CP contact times for ^{13}Cα and ^{13}C$'$ transfers were set to 2916 and 2694 μs, respectively. For heteronuclear decoupling CW (continuous wave) or TPPM (two pulse phase modulation),[35] ^{1}H RF amplitude was set to 100 kHz. DARR mixing was applied for 20 ms with ^{1}H RF amplitude was set to 13 kHz (ω_r). For the 2D MEIOSIS experiment, t_1 dwell time (dw) of 36 μs and 288 μs were respectively used for ^{13}C and ^{15}N indirect evolutions. The numbers of increments (ni) and transients (nt) are optimized such that the product of "ni" and "nt" is constant for ^{13}C and ^{15}N t_1 evolutions represented by t_1' and t_1'', respectively; $ni(t_1') = 128$, $nt(t_1') = 96$, $ni(t_1'') = 32$, and $nt(t_1'') = 384$ that gives the total t_1 evolution times of 4.57 and 8.92 ms for ^{13}C and ^{15}N, respectively.[9,10] For conventional experiments (Fig. 1S) $dw(t_1')$, $dw(t_1'')$, $ni(t_1')$, and $ni(t_1'')$ are identical to MEIOSIS; whereas the number of transients for DARR, N(CA)CX, CA(N)CO, and NCO were, respectively, set to 48, 152, 192, and 24. A recycle delay of 2 s was used in all experiments. For 3D MEIOSIS experiments, each of the indirect dimensions t_1 and t_2 use 21 increments, and a total of 56 scans were used. The dwell times of ^{13}C and ^{15}N were set to 150 and 300 μs, respectively, which

corresponds to total evolution times of 3 and 6 ms for ^{13}C and ^{15}N, respectively. The ^{13}C offset was centered at 60 ppm and the offset was moved to 170 ppm for $^{13}C'$ evolution during t_2''. This offset switching is achieved by phase modulation of ϕ_3 in synchrony with t_2'' evolution. The effective number of scans in 2D and 3D MEIOSIS experiments is twice the set number of scans (nt) due to the fact that two separate experiments are recorded with ^{15}N phase +x and −x, respectively, which are then constructively added to obtain individual pathways. Therefore, we compare MEIOSIS to the conventional methods using the total experimental time required to collect the data rather than number of scans. The ^{13}C spectra were referenced with respect to CH_2 resonance of adamantane at 40.48 ppm and indirectly to ^{15}N using relative gyromagnetic ratio of ^{15}N and ^{13}C.

Possible drawbacks for the implementation of the MEIOSIS scheme may result from the increase of the RF duty cycles. However, we have found that, the performance of the pulse sequences described here is well within the capabilities of commercial ssNMR probes.

ACKNOWLEDGMENTS

The authors would like to thank Frank (Fa-An) Chao for preparation of the labeled ubiquitin sample. This work is supported by the National Institutes of Health (GM64742 to GV).

[1]A. McDermott, Annu. Rev. Biophys. **38**, 385 (2009).
[2]S. R. Hartmann and E. L. Hahn, Phys. Rev. **128**, 2042 (1962).
[3]M. H. Levitt, D. Suter, and R. R. Ernst, J. Chem. Phys. **84**, 4243 (1986).
[4]J. Schlagnitweit, G. Zuckerstätter, and N. Müller, Magn. Reson. Chem. **48**, 1 (2010).
[5]T. Gopinath, R. Verardi, N. J. Traaseth, and G. Veglia, J. Phys. Chem. B **114**, 5089 (2010).
[6]T. Gopinath and G. Veglia, J. Am. Chem. Soc. **131**, 5754 (2009).
[7]T. Gopinath, N. J. Traaseth, K. Mote, and G. Veglia, J. Am. Chem. Soc. **132**, 5357 (2010).
[8]T. Gopinath, K. R. Mote, and G. Veglia, J. Chem. Phys. **135**, 074503 (2011).
[9]T. Gopinath and G. Veglia, Angew. Chem., Int. Ed. **51**, 2731 (2012).
[10]T. Gopinath and G. Veglia, J. Magn. Reson. **220**, 79 (2012).
[11]J. R. Banigan and N. J. Traaseth, J. Phys. Chem. B **116**, 7138 (2012).
[12]E. Kupce, L. E. Kay, and R. Freeman, J. Am. Chem. Soc. **132**, 18008 (2010).
[13]M. Fukuchi, M. Inukai, K. Takeda, and K. Takegoshi, J. Magn. Reson. **194**, 300 (2008).
[14]K. Schmidt-Rohr and H. W. Spiess, *Multidimensional Solid-State NMR and Polymers* (Academic Press, San Diego, 1994).
[15]K. Takegoshi, S. Nakamura, and T. Terao, Chem. Phys. Lett. **344**, 631 (2001).
[16]J. Pauli, M. Baldus, B. van Rossum, H. de Groot, and H. Oschkinat, Chem. Biol. Chem. **2**, 272 (2001).
[17]F. Castellani, B. van Rossum, A. Diehl, M. Schubert, K. Rehbein, and H. Oschkinat, Nature (London) **420**, 98 (2002).
[18]W. T. Franks, K. D. Kloepper, B. J. Wylie, and C. M. Rienstra, J. Biomol. NMR **39**, 107 (2007).
[19]M. Baldus, A. T. Petkova, J. Herzfeld, and R. G. Griffin, Mol. Phys. **95**, 1197 (1998).
[20]A. Pines, M. G. Gibby, and J. S. Waugh, J. Chem. Phys. **59**, 569 (1973).
[21]T. Gopinath and G. Veglia, Chem. Phys. Lett. **494**, 104 (2010).
[22]R. Verel, M. Ernst, and B. H. Meier, J. Magn. Reson. **150**, 81 (2001).
[23]M. Hohwy, C. M. Rienstra, C. P. Jaroniec, and R. G. Griffin, J. Chem. Phys. **110**, 7983 (1999).
[24]G. De Paepe, J. R. Lewandowski, A. Loquet, A. Bockmann, and R. G. Griffin, J. Chem. Phys. **129**, 245101 (2008).
[25]A. Brinkmann and M. H. Levitt, J. Chem. Phys. **115**, 357 (2001).
[26]C. Kehlet, M. Bjerring, A. C. Sivertsen, T. Kristensen, J. J. Enghild, S. J. Glaser, N. Khaneja, and N. C. Nielsen, J. Magn. Reson. **188**, 216 (2007).
[27]G. De Paepe, J. R. Lewandowski, A. Loquet, M. Eddy, S. Megy, A. Bockmann, and R. G. Griffin, J. Chem. Phys. **134**, 095101 (2011).
[28]P. Bellstedt, C. Herbst, S. Häfner, J. Leppert, M. Görlach, and R. Ramachandran, J. Biomol. NMR **54**, 325 (2012).
[29]A. Marchetti, S. Jehle, M. Felletti, M. J. Knight, Y. Wang, Z. Q. Xu, A. Y. Park, G. Otting, A. Lesage, L. Emsley, N. E. Dixon, and G. Pintacuda, Angew. Chem., Int. Ed. **51**, 10756 (2012).
[30]B. Reif, J. Magn. Reson. **216**, 1 (2012).
[31]T. Maly, G. T. Debelouchina, V. S. Bajaj, K. N. Hu, C. G. Joo, M. L. Mak-Jurkauskas, J. R. Sirigiri, P. C. A. van der Wel, J. Herzfeld, R. J. Temkin, and R. G. Griffin, J. Chem. Phys. **128**, 052211 (2008).
[32]N. P. Wickramasinghe, S. Parthasarathy, C. R. Jones, C. Bhardwaj, F. Long, M. Kotecha, S. Mehboob, L. W. M. Fung, J. Past, A. Samoson, and Y. Ishii, Nat. Methods **6**, 215 (2009).
[33]E. K. Paulson, C. R. Morcombe, V. Gaponenko, B. Dancheck, R. A. Byrd, and K. W. Zilm, J. Am. Chem. Soc. **125**, 15831 (2003).
[34]A. B. Nielsen, K. Szekely, J. Gath, M. Ernst, N. C. Nielsen, and B. H. Meier, J. Biomol. NMR **52**, 283 (2012).
[35]A. E. Bennett, C. M. Rienstra, M. Auger, K. V. Lakshmi, and R. G. Griffin, J. Chem. Phys. **103**, 6951 (1995).
[36]See supplementary material at http://dx.doi.org/10.1063/1.4803126 for Figs. 1S–4S.